Inorg. Chem. **2008**, *47*, 9103−9110

Spontaneous Magnetization in Ni−Al and Ni−Fe Layered Double Hydroxides

Eugenio Coronado, José R. Galán-Mascarós,* Carlos Martí-Gastaldo, Antonio Ribera,* Elías Palacios, Miguel Castro, and Ramón Burriel

Instituto de Ciencia Molecular, Universidad de Valencia, Polígono de la Coma, s/n, 46980 Paterna, Spain, and Instituto de Ciencia de Materiales de Aragón, CSIC - Universidad de Zaragoza, Plaza San Francisco s/n, 50009 Zaragoza, Spain

Received June 17, 2008

Layered double hydroxides containing paramagnetic Ni^{II} and diamagnetic/paramagnetic Al^{III}/Fe^{III} ions have been prepared and characterized. $Ni_2Al(OH)_6(NO_3)\cdot nH_2O$ (**1**), $Ni_2Fe(OH)_6(NO_3)\cdot nH_2O$ (**2**), $Ni_2Fe(OH)_6(C_6H_8O_4)_{0.5}\cdot nH_2O$ (**3**), and $Ni_2Fe(OH)_6(C_{10}H_{16}O_4)_{0.5}\cdot nH_2O$ (**4**) were prepared by coprecipitation at controlled pH as polycrystalline materials with the typical brucite-like structure, with alternating layers of hydroxide and the corresponding anions, which determine the interlayer separation. Magnetic studies show the appearance of spontaneous magnetization between 2 and 15 K for these compounds. Interestingly, the onset temperature for spontaneous magnetization follows a direct relationship with interlayer separation, since this is the only magnetic difference between compounds **2**, **3**, and **4**. Magnetic and calorimetric data indicate that long-range magnetic ordering is not occurring in any of these materials, but rather a freezing of the magnetic system in 3D due to the magnetic disorder and competing intra- and interlayer interactions. Thus, these hydrotalcite-like magnetic materials can be regarded as spin glasses.

Introduction

Layered double hydroxides (LDHs) have been the object of many studies for decades,[1] mostly due to their remarkable potential technological applications.[2–4] These synthetic anionic clays, having a hydrotalcite-like structure, possess exchangeable anions located in the interlayer spaces to compensate for the positive charge of the brucite-type hydroxide layers. The chemical composition of LDHs follows the formula $[M^{II}_{(1-x)}M^{III}_x(OH)_2][A^{n-}_{(x/n)}(H_2O)]$ (M^{II} = Mg, Co, Ni, Zn,...; M^{III} = Al, Cr, V, Ga, Rh,...). A^{n-} is the charge compensating anion. A large variety of anions have been successfully inserted into LDHs, from simple (CO_3^{2-}, NO_3^-) to really complex molecules, such as polyoxometallates, macrocyclic ligands, nucleosides, or even DNA.[5–7] Their high surface area, the control over composition, and their anion exchange properties make LDHs increasingly interesting in a variety of areas such as adsorbents,[8,9] ion exchangers,[10,11] modified electrodes,[12–14] catalysis,[15–18] and medical

* Authors to whom correspondence should be addressed. Phone: 34-963544420. Fax: +34-963543273. E-mail: alan@uv.es.

(1) *Layered Double Hydroxides: Present and Future*; Rives, V., Ed.; Nova Science Publishers: New York, 2001. and refs therein.
(2) Leroux, F.; Besse, J. P. In *Clay Surfaces: Fundamentals and Applications*; Wypych, F., Satyanarayana, K. G., Eds.; Elsevier: London, 2004; pp 459−495.
(3) de Roy, A.; Forano, C.; El Malki, K.; Besse, J. P. In *Expanded Clays and other Microporous Solids*; Occelli, M. L., Robson, H. E., Eds.; Van Nostrand Reinhold: New York, 1992.
(4) Feng, L.; Duan, X. *Struct. Bonding (Berlin)* **2006**, *119*, 193–223.
(5) Newman, S. P.; Jones, W. *New J. Chem.* **1998**, *22*, 105–110.
(6) Rives, V.; Ulibarri, M. A. *Coord. Chem. Rev.* **1999**, *181*, 61–120.
(7) Choy, J. H.; Kwak, S. Y.; Park, J. S.; Jeong, Y. J.; Portier, J. *J. Am. Chem. Soc.* **1999**, *121*, 1399–1400.
(8) You, Y. W.; Zhao, H. T.; Vance, G. F. *J. Mater. Chem.* **2002**, *12*, 907–912.
(9) Jin, S.; Fallgren, P. H.; Morris, J. M.; Chen, Q. *Sci. Tech. Adv. Mater.* **2007**, *8*, 67–70.
(10) Meyn, M.; Beneke, K.; Lagaly, G. *Inorg. Chem.* **1993**, *32*, 1209–1215.
(11) Millange, F.; Walton, R. I.; Lei, L. X.; O'Hare, D. *Chem. Mater.* **2000**, *12*, 1990–1994.
(12) Jayashree, R. S.; Kamath, P. V. *J. Power Sources* **2002**, *107*, 120–124.
(13) Qiu, J. B.; Villemure, G. J. *Electroanal. Chem.* **1997**, *428*, 165–172.
(14) Ehlsissen, K. T.; Delahayevidal, A.; Genin, P.; Figlarz, M.; Willmann, P. *J. Mater. Chem.* **1993**, *3*, 883–888.
(15) Sels, B. F.; De Vos, D. E.; Jacobs, P. A. In *Catalysis Reviews: Science and Engineering*; Taylor & Francis Group: New York, 2001; pp 443−488.
(16) Sels, B.; De Vos, D.; Buntinx, M.; Pierard, F.; Kirsch-De Mesmaeker, A.; Jacobs, P. *Nature* **1999**, *400*, 855–857.
(17) Choudary, B. M.; Madhi, S.; Chowdari, N. S.; Kantam, M. L.; Sreedhar, B. *J. Am. Chem. Soc.* **2002**, *124*, 14127–14136.

10.1021/ic801123v CCC: $40.75
Published on Web 08/06/2008

applications.[19,20] In this vein, magnetic clays could have remarkable added value in the technology of adsorbants, catalysts, or ion exchangers as they will be able to attract, separate, or manipulate them by magnetic fields.

Few studies have been made on the magnetic properties of LDHs,[21,22] despite the fact that remarkable magnetic phenomena could be encountered. These expectations can be derived from a comparison with those found in the series of homometallic layered hidroxides, which show huge magnetic coercivity.[23–25] Although in LDHs the random distribution of the paramagnetic species makes the analysis of the data a more difficult task, they could offer some advantages with respect to these layered hydroxides, such as better crystallinity, tunability of the magnetic properties, and, in addition, all the intrinsic properties of LDHs, including anion exchange, as a new class of multifunctional materials.

Regarding magnetic LDHs, only the magnetism of $Co_2Fe_yAl_{(1-y)}(OH)_6Cl\cdot nH_2O$ has been loosely investigated,[21] in samples with interlayer spacings between 7.6 and 25 Å. It was reported that the low-temperature regime and the apparent magnetic ordering were affected by the interlayer separation, without any detailed conclusions. This is another interesting characteristic for LDHs: their lamellar structure. The anionic spacer determines the interlayer separation, and therefore, it offers a perfect strategy for the study of the effect of dimensionality on magnetic properties by controlling the interlayer separation when changing the spacer, while maintaining the magnetic network.

In general, magnetic LDHs have been mostly studied as precursors for metal oxides, since their thermal decomposition leads to the formation of mixed metal oxides with a high metal dispersion and high surface area.[26,27] On the other hand, the insertion of magnetic anions into the interlaminar space has usually been studied with nonmagnetic or paramagnetic LDHs. In this way, polyoxometallates,[28] nitronyl nitroxides,[29] and homo- and heterometallic oxalate complexes[30–33] have been embedded into LDH frameworks. No effects upon the magnetic properties were observed due to the confinement of the molecules.

We present here the synthesis and complete characterization of a family of Ni−Fe LDHs, with different anionic spacers: nitrate, adipate, and sebacate. In this family of formula $[Ni_2Fe(OH)_6][A^{n-}]_{\{1/n\}}$, A = NO_3^-, $C_6H_8O_4^{2-}$, and $C_{10}H_{16}O_4^{2-}$, the hydroxide layers are identical from one material to another, but different spacings are reached by changing the anions. Remarkable effects upon the magnetic properties are observed, while the magnetic nature goes from 3D to quasi-2D character.

Experimental Section

Synthesis. The following analytical-grade chemicals were purchased from Sigma-Aldrich and used without further purification: NaOH, $Ni(NO_3)_2\cdot 6H_2O$, $Fe(NO_3)_3\cdot 9H_2O$, $Al(NO_3)_3\cdot 9H_2O$, $NaNO_3$, $HO_2C(CH_2)_4CO_2H$ (adipic acid), and $HO_2C(CH_2)_8CO_2H$ (sebacic acid). All manipulations were carried out under an inert atmosphere in order to avoid the carbonate anions.

$Ni_2M(OH)_6(NO_3)\cdot nH_2O$. NiAl−$NO_3$ (M = Al^{III}, **1**) and NiFe−NO_3 (M = Fe^{III}, **2**) were prepared in a 2:1 molar ratio from their respective nitrate salts, in an excess of nitrate, so that the nitrate was the only anion present at the interlaminar space. The above samples were prepared by coprecipitation, following the Miyata method[34] at constant pH. In this method, two solutions (a 1 M solution of Ni^{II} and M^{III} and a 1 M solution of NaOH and $NaNO_3$) were added dropwise while stirring at room temperature. The amount of each solution was fixed by the expression $Ni^{II}_2M^{III}(OH)_6(NO_3)_4$, keeping the pH = 8 for **1** and pH = 7 for **2**. After the mixing process was finished, the resulting slurry was kept 1 h more at room temperature and later on heated at 353 K at atmospheric pressure and without stopping the stirring. The gel was aged over 5 days and finally filtered, washed throughout with distilled and decarbonated water until an absence of nitrate was reached, and dried at room temperature under a vacuum.

$Ni_2Fe(OH)_6(carboxylate)_{0.5}\cdot nH_2O$. NiFe−Adi (adipate, **3**) and NiFe−Seb (sebacate, **4**) were prepared by an analogous procedure to that described for the nitrate anions, just taking into account that these acids will be incorporated into the LHDs as divalent anions. Thus, the $Ni^{II}_2Fe^{III}(OH)_6$(adipate/sebacate)$_2$ expression was used instead for the solutions to be mixed dropwise. The NaOH/adipate or sebacate solution was prepared in situ from adipic or sebacic acid, respectively. The resulting slurries with a pH = 7 were kept at room temperature for 1 h after finishing the mixing, and later on, the temperature was increased to 353 K. The gel was aged over 5 days and finally filtered, washed, and dried as already described.

Analysis and X-Ray Diffraction (XRD). Elemental analysis electron probe microanalysis (EPMA) was performed on a Philips SEM-515. A thermogravimetry analysis was performed in a Mettler Toledo TGA/SDTA 851 apparatus in the 25−800 °C temperature range under 30 mL min^{-1} of air flow and at a 10 K min^{-1} scan rate. X-ray powder diffraction data were collected on a Siemens D-500 X-ray powder diffractometer with Cu K_α radiation (λ = 1.5418 Å) and with a rotating anode D-max Rigaku at 80 mA and 45 kV. Samples were mounted on a flat sample plate. Profiles were collected in the 2.5° < 2θ < 90° range with a step size in the 0.05−0.03° range at 1 step/s.

(18) Cervilla, A.; Corma, A.; Fornes, V.; Llopis, E.; Palanca, P.; Rey, F.; Ribera, A. *J. Am. Chem. Soc.* **1994**, *116*, 1595–1596.
(19) Xu, Z. P.; Lu, G. Q. *Pure Appl. Chem.* **2006**, *78*, 1771–1779.
(20) Choy, J. H.; Jung, J. S.; Oh, J. M.; Park, M.; Jeong, J.; Kang, Y. K.; Han, O. J. *Biomaterials* **2004**, *25*, 3059–3064.
(21) Intissar, M.; Segni, R.; Payen, C.; Besse, J.-P.; Leroux, F. *J. Solid State Chem.* **2002**, *167*, 508–516.
(22) Morlat-Thérias, S.; Mousty, C.; Palvadeau, P.; Molinié, P.; Léone, P.; Rouxel, J.; Taviot-Guého, C.; Ennaqui, A.; de Roy, A.; Besse, J. P. *J. Solid State Chem.* **1999**, *144*, 143–151.
(23) Taibi, M.; Ammar, S.; Jouini, N.; Fiévet, F.; Molinié, P.; Drillon, M. *J. Mater. Chem.* **2002**, *12*, 3238–3244.
(24) Huang, Z. L.; Drillon, M.; Masciocchi, N.; Sironi, A.; Ahzo, J. T.; Rabu, P.; Panissod, P. *Chem. Mater.* **2000**, *12*, 2805–2812.
(25) Kurmoo, M. *Chem. Mater.* **1999**, *11*, 3370–3378.
(26) Li, F.; Liu, X. F.; Yang, Q. Z.; Liu, J. J.; Evans, D. G.; Duan, X. *Mater. Res. Bull.* **2005**, *40*, 1244–1255.
(27) Li, F.; Liu, J. J.; Evans, D. G.; Duan, X. *Chem. Mater.* **2004**, *16*, 1597–1602.
(28) Yun, S. K.; Pinnavaia, T. J. *Inorg. Chem.* **1996**, *35*, 6853–6860.
(29) Caneschi, A.; Gatteschi, D.; Sangregorio, C.; Vaz, M. G. F.; Costantino, U.; Nocchetti, M.; Vivani, R. *Inorg. Chim. Acta* **2002**, *338*, 127–132.
(30) Prevot, V.; Forano, C.; Besse, J. P. *J. Mater. Chem.* **1999**, *9*, 155–160.
(31) Prevot, V.; Forano, C.; Besse, J. P. *J. Solid State Chem.* **2000**, *153*, 301–309.
(32) del Arco, M.; Gutiérrez, S.; Martín, C.; Rives, V. *Inorg. Chem.* **2003**, *42*, 4232–4240.
(33) Coronado, E.; Galán-Mascarós, J. R.; Martí-Gastaldo, C.; Ribera, A. *Chem. Mater.* **2006**, *18*, 6112–6114.
(34) Miyata, S. *Clays Clay Miner.* **1980**, *28*, 50–56.

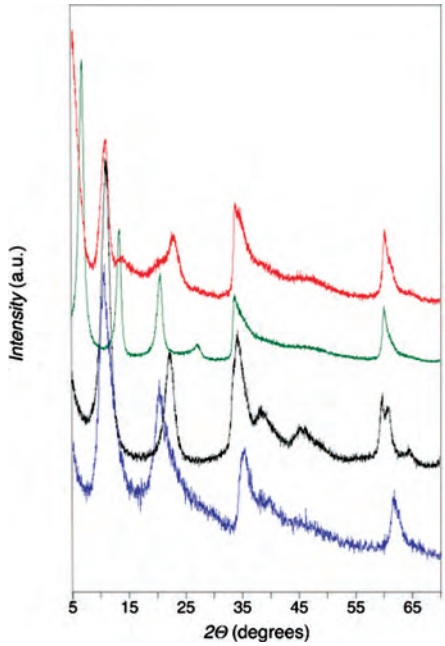

Figure 1. X-ray powder diffraction patterns for $NiAl-NO_3$ (**1**, blue), $NiFe-NO_3$ (**2**, black), NiFe−Adi (**3**, green), and NiFe−Seb (**4**, red).

Physical Measurements. Magnetic measurements were carried out with a Quantum Design (SQUID) Magnetometer MPMS-XL-5. The susceptibility data were corrected for the diamagnetic contributions calculated using the Pascal constants. The dc data were collected with an applied field of 1000 G (10^{-1} T) in the 2−300 K temperature range, and magnetization studies were performed between −5 and +5 T at 2 K. The ac data were collected in the 2−20 K range with an applied alternating field of 3.95 G (0.395×10^{-3} T) at different frequencies in the 1−997 Hz range.

Results and Discussion

Synthesis and Structure. All compounds, $NiAl-NO_3$ (**1**), $NiFe-NO_3$ (**2**), NiFe−Adi (**3**), and NiFe−Seb (**4**), were prepared according to the method proposed by Miyata,[35] yielding a green powder for **1**, and yellow-brown powders for **2**−**4**. We would like to remark on the importance of keeping a constant pH value (around 7) during the synthesis procedure for the NiFe-LDHs. Higher pH values gave other solid phases different that LDH, which could be easily identified because they behave as permanent magnets at room temperature. An XRD analysis of these samples corroborated this fact.

The X-ray powder data for all samples obtained (Figure 1) indicate that all materials have reasonably good crystallinity and purity, with an estimated diameter between 100 and 260 Å for the crystallites. Only LDH materials are present; no other phase was observed. The indexation of the peaks as (001), by assuming the rhombohedral symmetry, as assigned by Miyata,[36] allowed us to determine the basal spacing in each case. The shift found in the peaks at lower angles corresponds to the increase in the interlayer separation, as the anion size changes. Because the van der Waals thickness of the brucite sheets is ca. 4.7 Å, the calculated basal spacing indicates a gallery height of ca. 3.5 and 3.7 Å for **1** and **2**, respectively, 8.49 Å for **3**, and 10.67 Å for **4**. Attending to the organic molecules' size, we consider that the dicarboxylates appear slightly tilted with respect to the *c* axis, with an angle of approximately 60° for **3** and 55° for **4**. This fact is in good agreement with that described in previously reported works concerning layered hydroxide salts.[37,38] In these works, the authors observed a linear increase of the basal spacing with the number of carbons of the intercalated organic molecule alkyllic chain and concluded that the alkyl chains are not perpendicular to the hydroxide-based plane but present a certain tilting angle with respect to the *c* axis.

The nature of the anionic intercalated moiety showed no influence on the in-plane intermetallic distance. Indeed, low-intensity reflections around 60°, indexed as (110), allowed for the estimation of the unit cell *a* parameters for all compounds (see Table 1). Clearly, the values for the NiFe−LDH's derivatives remain constant around 1.54 Å. On the other hand, a slightly smaller *a* value is obtained for **1**. This diminution must be related to the smaller Al^{III} ionic radius (0.535 Å) if compared to the Fe^{III} one (0.645 Å).[39]

In the hexagonal anionic layer built from edge-sharing metallic octahedra, a random distribution of metal ions will be present according to the found stoichiometry (Table 2). For NiAl−LDH, this means that, statistically, each Ni atom will have an average of three neighboring Ni atoms, but with nonzero probabilities to have any given number between zero and six. In NiFe−LDH, the network of Ni atoms will be identical. The paramagnetic Fe^{III} centers present in these materials are a minority, and they will occupy statistically three (non-adjacent) of the six nearest neighbors of the Ni^{II} octahedra, while each Fe^{III} octahedron will be statistically surrounded by six Ni^{II} centers. It is important to take into account that the probability of Fe−O−Fe pairs is very low, but nonzero, and a given quantity of these pairs will be randomly distributed throughout the layers.

Thermogravimetric/differential thermal analysis (TG/DTA) curves obtained for **1**−**4** under an air atmosphere in the 25−800 °C range (Figures S2−S5, Supporting Information) present a first weight loss region (90−200 °C) that corresponds to the removal of surface and intercalated water accompanied by a broad, poorly defined endothermic peak in the DTA curve. A second weight loss is observed in the temperature range 200−450 °C that corresponds to intercalated anion decomposition and further dehydroxylation of the brucitelike sheets. While for compounds **1** and **2** this second weight loss is certified by the presence of an endothermic peak in the DTA thermogram, as usually observed for LDH,[40] **3** and **4** simultaneously exhibit a strong exothermic peak in the same temperature range, thus hiding the typically observed endothermic event. This exothermic

(35) Miyata, S. *Clay Miner.* **1980**, *19*, 591–596.
(36) Miyata, S.; Okada, A. *Clays Clay Miner.* **1977**, *25*, 14–18.
(37) Meyn, M.; Beneke, K.; Lagaly, G. *Inorg. Chem.* **1993**, *32*, 1209–1215.
(38) Rabu, P.; Drillon, M.; Awaga, K.; Fujita W.; Sekine, T. In *Magnetism: Molecules to Materials II*; Miller, J. S., Drillon, M., Eds.; Wiley VCH: Weinheim, Germany, 2001; p 357.
(39) Shannon, R. D. *Acta Crystallogr.* **1976**, *32*, 751–767.

Table 1. Main Peaks and Calculated Basal Spacing from the Powder X-Ray Diffraction Pattern of NiAl−NO_3 (**1**), NiFe−NO3 (**2**), NiFe−Adi (**3**), and NiFe−Seb (**4**)

	hkl = 003		hkl = 006		hkl = 009		hkl = 110		estimated parameters		
	2Θ °	d (Å)	2Θ °	d (Å)	2Θ °	d (Å)	2Θ °	d (Å)	a^a (Å)	c^b (Å)	BS^c (Å)
1	10.50	8.42	20.24	4.39			61.74	1.50	3.00	25.8	8.60
2	11.15	7.94	22.40	3.97			60.00	1.54	3.07	23.82	7.94
3	6.70	13.19	13.40	6.61	20.75	4.28	60.19	1.54	3.07	39.25	13.08
4	5.75	15.37	11.55	7.66	17.20	5.16	60.26	1.54	3.07	46.17	15.39

[a] $a = 2d_{(110)}$. [b] $c = (c_{003} + c_{006} + c_{009})/3$. [c] BS = $c/3$.

Table 2. Elemental Chemical Analysis Data for NiAl−NO_3 (**1**), NiFe−NO_3 (**2**), NiFe−Adi (**3**), and NiFe−Seb (**4**)[a]

M(II)/M(III)[b]			water content[c]		
sample	exp.	synth.	weight loss	molecules	molecular formula
1	1.63	2	11.22	1.8	$[Ni_{1.86}Al_{1.14}(OH)_6](NO_3)_{1.14}\cdot 1.8H_2O$
2	2.00	2	14.53	3.2	$[Ni_2Fe(OH)_6](NO_3)\cdot 3.2H_2O$
3	1.94	2	14.88	3.4	$[Ni_{1.98}Fe_{1.02}(OH)_6](C_6H_8O_4)_{0.5}\cdot 3.4H_2O$
4	2.19	2	16.71	4.2	$[Ni_{2.06}Fe_{0.94}(OH)_6](C_6H_8O_4)_{0.5}\cdot 4.2H_2O$

[a] Weight percentage estimated from elemental analysis. [b] Molar ration between metallic ions (M^{III} = Al, Fe; M^{II} = Ni) obtained from EPMA. [c] Water content extracted from TG analysis.

signal must be related to the catalytic oxidation of carbon organic species in the presence of generated nickel oxide.[41]

Although we did not monitor the gas evolution and composition during the thermal decomposition process, water content in the studied samples can be extracted from the first weight loss step (Table 2). In view of the obtained results, compound **1** contains fewer water molecules than **2**, and then the water content increased in **3** and **4**, as expected for their larger interplane distances between brucite-like sheets in the pillared solid state.

FT-IR spectroscopy is a very useful technique in the study of LDH. It not only allows for the identification of molecules intercalated in the LDH interlaminar space but is helpful as well in the study of their orientation with respect to the brucite-like sheets. Important information about the interaction of interlaminar anions, in terms of nature and intensity, with the neighboring hydroxo groups can also be extracted. Figure S1 (Supporting Information) shows the FT-IR recorded spectra for compounds **1**−**4**. The broad intense lines observed between 3416 and 3388 cm^{-1} are ascribed to the O−H stretching vibration mode of water molecules intercalated within the interlaminar space. Besides interlaminar water molecules, hydrogen-bonded hydroxyl groups along the cationic sheets might also be responsible for the band broadening. The medium-intensity band around 1630 cm^{-1} is related to hydrogen-bonded water molecules' bending mode. In fact, this band intensity is proportional to the amount of intercalated water in the studied sample. CO_3^{2-} anions' stretching mode (ν^3) is responsible for the sharp strong band around 1360 cm^{-1}. Stretching and bending

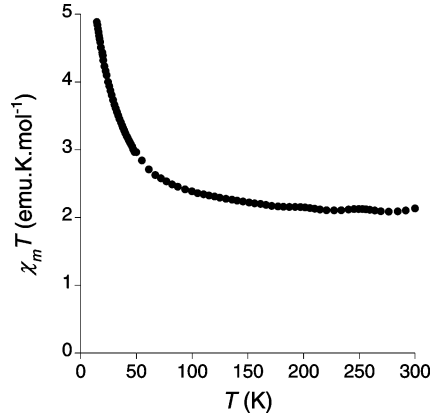

Figure 2. Temperature dependence of the χT product for NiAl−NO_3 (**1**).

vibrational modes attributed to hydroxometallic octahedral complexes constituting the $[Ni^{II}_{1-x}Cr^{III}_x(OH)_2]^{x+}$ (M = Al, Fe) cationic brucitelike sheets are responsible for absorption at lower wavenumbers.

Magnetic Properties. The magnetic properties of **1** were studied first to determine the Ni−O−Ni magnetic interactions present in all of these materials, where the paramagnetic Fe^{III} was substituted by the diamagnetic Al^{III}, while maintaining the same crystal structure. As discussed earlier, although the metallic random distribution in the layers will affect the local magnetic environment of individual Ni^{II} ions, in all cases, superexchange must occur through the oxo bridges between adjacent NiO_6 octahedra-sharing edges. The Ni−O−Ni angle in this type of structure should be close to 90°, favoring orthogonality of the Ni^{II} magnetic orbitals. In model compounds, this situation usually promotes ferromagnetic exchange,[42] as it was also observed for the brucite-type layered nickel hydroxide.[23] Indeed, the χT product for **1** (Figure 2) increases continuously when the temperature is decreased from its room temperature value (χT_{rt} = 2.29 emu K mol^{-1}). This value is in good agreement with the expected spin-only value (Table 3). From the fitting of the high-temperature data to a Curie−Weiss law, we can estimate a Weiss constant θ = +14.5 K, confirming the presence of ferromagnetic interactions between Ni^{II} centers. Below 50 K, the magnetic moment starts to increase very rapidly, suggesting the presence of cooperative interactions. At 3.8 K (Figure 3), the out-of-phase ac magnetic susceptibility becomes nonzero,

Table 3. Main Magnetic Data and Parameters for NiAl−NO_3 (**1**), NiFe−NO_3 (**2**), NiFe−Adi (**3**), and NiFe−Seb (**4**)

sample	χT_{rt}	C (emu K mol^{-1})	C_{SO} (emu K mol^{-1})	θ (K)	TIP	T_C (K)	M_S (μ_B)	M_R (μ_B)	H_{Coer} (kG)
1	2.29	1.99	1.86	14.5	3.3×10^{-4}	3.8	2.63	0.16	0.13
2	7.78	7.13	6.375	31.99	2.4×10^{-3}	14.5	3.05	0.95	3.96
3	7.64	7.47	6.44	5.61	2.6×10^{-3}	12.5	3.77	0.03	<0.1
4	5.98	6.01	6.173	−2.67	2.32×10^{-4}	11	3.34	0.04	0.2

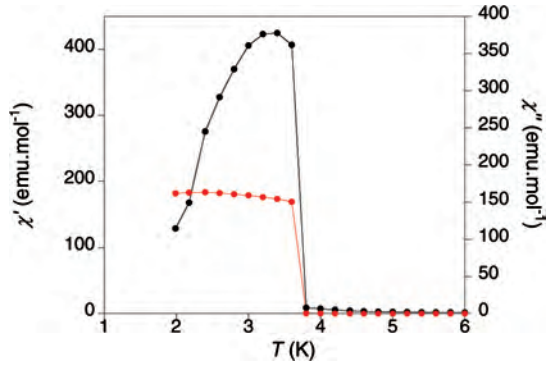

Figure 3. Temperature dependence of the ac magnetic susceptibilities for $NiAl-NO_3$ (**1**): in-phase χ' (black) and out-of-phase χ'' (red).

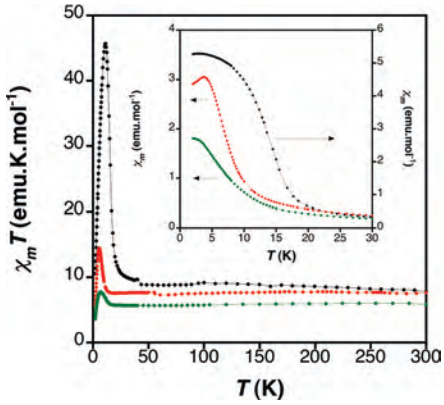

Figure 4. Temperature dependence of the dc χT product for $NiFe-NO_3$ (**2**, black), NiFe−Adi (**3**, green), and NiFe−Seb (**4**, red).

a signature of the onset spontaneous magnetization, and no significant frequency dependence of the ac susceptibility peaks was observed. A hysteresis loop with a coercive field, $H_C = 130$ G, was found at 2 K.

The magnetic moments at room temperature for the NiFe compounds (Figure 4) show also values in good agreement with that expected for the spin-only value for one high-spin Fe^{III} and two Ni^{II}'s (Table 3). The high-temperature regime can also be fitted to a Curie−Weiss law, giving Curie constants of 7.13, 7.47, and 6.01 emu K mol^{-1} for **2**, **3**, and **4**, respectively, and Weiss constants that become more negative as the interlayer separations becomes wider: from 31.99 K in **2**, to 5.61 K in **3**, and down to −2.67 K in **4**. This suggests that the interlayer interactions, which must become weaker through the series, are actually ferromagnetic, while the intralayer interactions show antiferromagnetic character, as expected. Although the Ni−O−Ni interaction will still be ferromagnetic, the presence of Fe−O−Ni pairs will promote antiferromagnetic coupling, since Fe^{III} has all of its d orbitals singly occupied, and therefore, mixing of the orbitals with the e_g magnetic orbitals of the Ni^{II} ions cannot be avoided. If we consider that all second neighbor interactions are negligible, the magnetic exchange in each layer will be dominated by the antiferromagnetic alignment of the noncompensating Ni^{II} and Fe^{III} subnetworks, with the magnetic moments aligned parallel to each other in each subnetwork. The apparently well-ordered magnetic network will be disrupted by the presence of randomly distributed Fe−O−Fe pairs. An antiferromagnetic Fe−O−Fe pair will

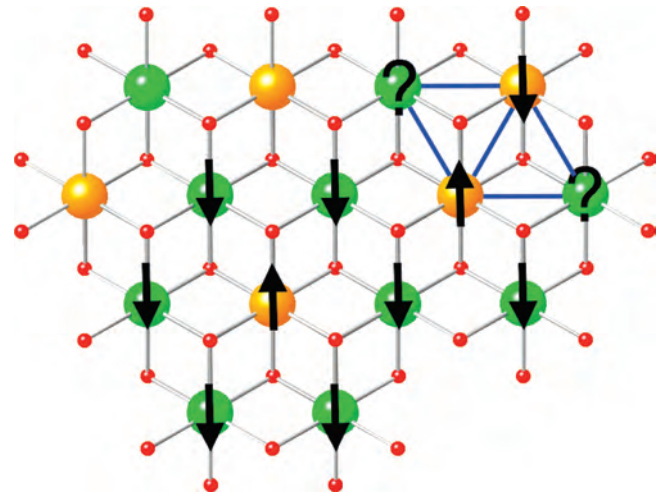

Figure 5. Random metal distribution in the brucitelike layer of NiFe−LDH's showing the possible appearance of spin frustration due to statistical disorder (Ni in green; Fe in yellow).

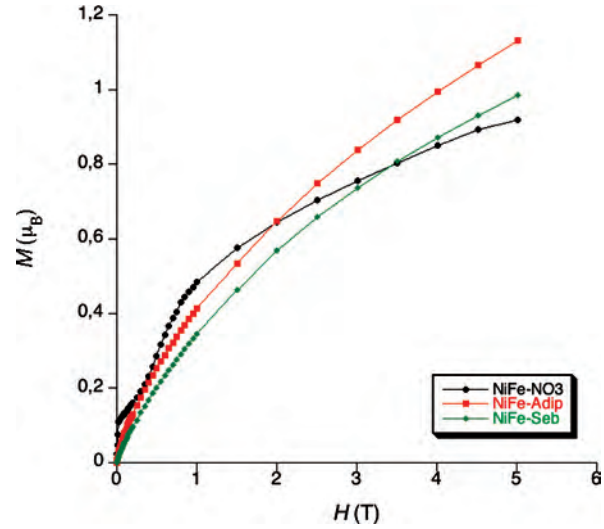

Figure 6. Field dependence of the magnetization for $NiFe-NO_3$ (**2**), NiFe−Adi (**3**), and NiFe−Seb (**4**).

generate spin frustration in the system, since the surrounding Ni^{II} ions connected to both Fe^{III} ions will tend to remain antiparallel to both of them (Figure 5). The overall magnetic properties in these materials will be determined finally by the interlayer interactions between these magnetic layers, separated from each other by the diamagnetic anions. At low temperatures, a pronounced increase in the magnetic susceptibility (Figure 4, inset) appears in all three cases, suggesting the appearance of spontaneous magnetization.

The predominance of antiferromagnetic interactions is confirmed by the field dependence of the magnetization at 2 K (Figure 6). It shows a continuous increase, but reaching values at 5 T far from saturation, as expected for ferrimagnetic systems (3.05, 3.88, and 3.34 μ_B for **2**, **3**, and **4**, in comparison with the expected saturation values of 9.00, 9.06, and 8.82 μ_B, respectively). In the case of **2**, it shows a very fast increase in the magnetization, reaching 0.1 μ_B, and then

(40) Kloprogge, J. T.; Frost, R. L. *Appl. Catal.* **1999**, *184*, 61–71.
(41) Poul, L.; Jouini, N.; Fiévet, F. *Chem. Mater.* **2000**, *12*, 3123–3132.
(42) Clemente-Juan, J. M.; Coronado, E.; Galán-Mascarós, J. R.; Gómez-García, C. J. *Inorg. Chem.* **1999**, *38*, 55–63.

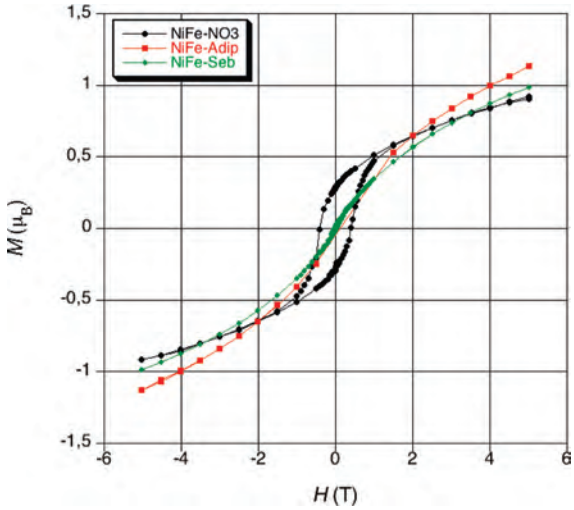

Figure 7. Hysteresis of the magnetization for NiFe−NO_3 (**2**), NiFe−Adi (**3**), and NiFe−Seb (**4**) at 2 K.

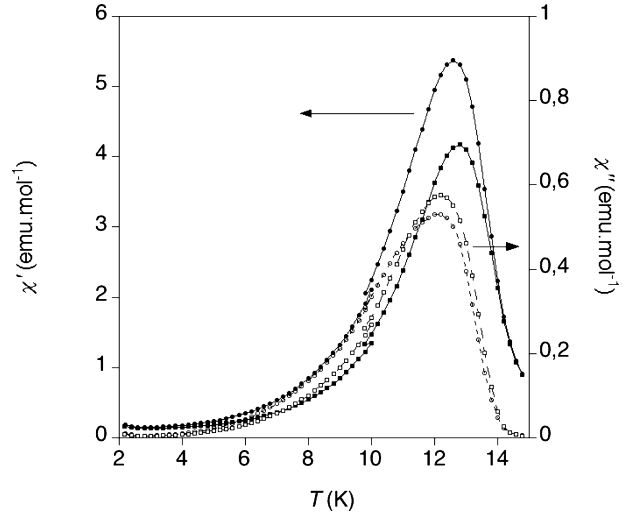

Figure 8. Temperature dependence of the ac magnetic susceptibility for NiFe−NO_3 (**2**) at 100 and 997 Hz (square and circle data points, respectively).

changes the slope following the expected pattern of slow increase up to 1 T (0.5 μ_B), where a second change in slope takes place, and the magnetization increases at an even slower pace. These features must be related to the smaller interlayer distances, in this case, and are therefore related to the interlayer interactions, although the complexity of the system prevents any further analysis.

Hysteresis loops (Figure 7) are observed at 2 K, confirming also the appearance of spontaneous magnetization in these materials, with its corresponding magnetic memory effect. The hysteresis loops decrease very rapidly as the basal spacing increases from 3960 Oe (**2**) to ∼100/200 Oe (**3** and **4**). This suggests that the domain movement is anchored by the interlayer interactions, yielding a magnetically harder material.

In agreement with these data, dynamic (ac) magnetic susceptibility measurements show a maximum in the in-phase susceptibility (χ') and the appearance of an out-of-phase signal (χ''). The temperature for the onset of spontaneous magnetization (T_M) can be defined as the temperature where χ'' becomes nonzero. Remarkably, while all dc measurements were analogous for all derivatives, a quite different ac magnetic behavior was found for **2**, **3**, and **4**, and not only with respect to the position of T_M. In the case of **2** (Figure 8), χ'' becomes nonzero at 14 K and shows a round peak at 12 K. Also χ' reaches a maximum just a few tenths of a Kelvin above the corresponding maximum observed for χ'', and in both cases, the peaks are relatively narrow (3 K width at half height).

In the case of **3** (Figure 9), the χ' peak becomes much wider, and its maximum moves down to 6 K, with the appearance of a small shoulder around 10 K. The out-of-phase signal becomes nonzero at 12 K, but instead of reaching a broad maximum, it starts to increase continuously, showing a small shoulder around 8 K, and reaching a rounded maximum around 4 K, far below the one observed in χ'. Thus, T_M decreases 2 K, when the interlayer separation goes from 7.94 up to 13.19 Å, but in addition, some further dynamic effects are occurring. Apparently, two different

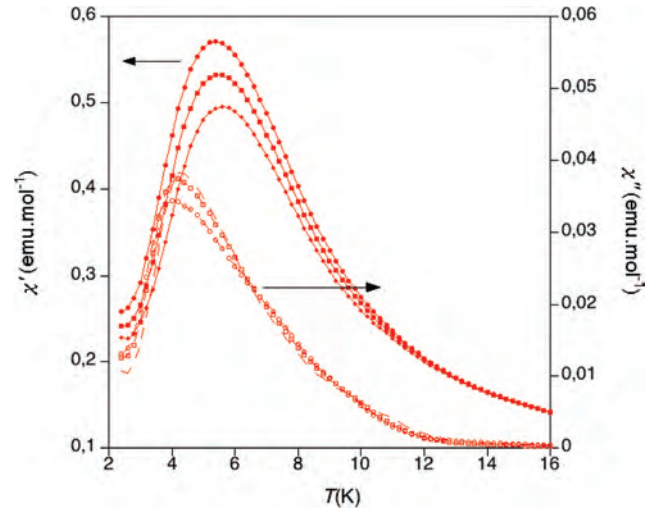

Figure 9. Temperature dependence of the ac magnetic susceptibility for NiFe−Adi (**3**) at 10, 100, and 997 Hz (rhomb, square, and circle data points, respectively).

processes are controlling the dynamics of the magnetization once the spontaneous magnetization is achieved.

The same tendency, but even more pronounced, is observed in **4** (Figure 10). In this case, two different anomalies are observed in χ', with one shoulder that appears at 11 K and one maximum around 4.5 K. These two peaks have their corresponding peaks in χ'', which become nonzero at 11.6 K, to reach a first maximum at 9.0 K and a second one at 3.5 K. As the interlayer separation increases from **2** to **4**, these data suggest that, in **2**, apparently a single process occurs, giving a single peak due to the 3D character, and the lowering of the dimensionality splits this peak in two different features, which appear very close in **3** and finally are clearly separated in **4**. The peak at higher temperatures is related to the appearance of spontaneous magnetization in these systems, and therefore the low-temperature peak must be related to dynamic processes, such as domain wall movement, that will be clearly related to the dimensionality of the system, where the isolation of the layers into quasi 2D networks will constrain the movement of

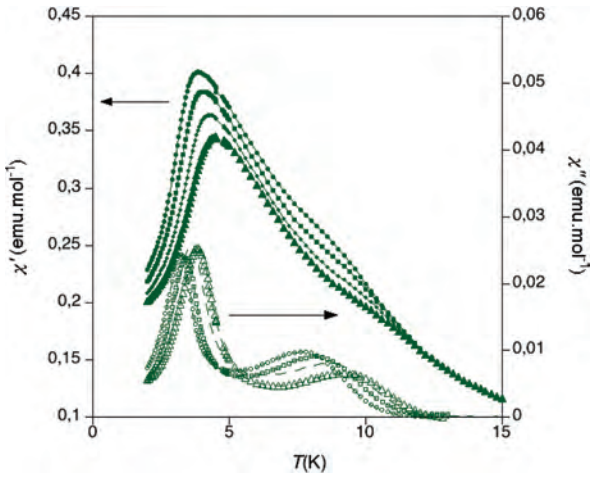

Figure 10. Temperature dependence of the ac magnetic susceptibility for NiFe−Seb (**4**) at 1, 10, 100, and 997 Hz (triangle, rhomb, square, and circle data points, respectively).

the magnetic domain walls, which will be forced to remain always in the plane.

A small frequency dependence is observed for all of the peaks found in the ac susceptibility data for the NiFe−LDH's, which can be an indication of glassy behavior. From this frequency dependence, the ϕ parameter (as a function of T_f: temperature of the maximum in χ'' for a given ω), as defined by Mydosh,[43] can be estimated:

$$\varphi = \Delta Tf/[T_f \Delta(\log \omega)] \quad (1)$$

The values for ϕ are in good agreement with those expected for spin glasses (0.020, 0.031, and 0.058 for **2**, **3**, and **4**, respectively; in a typical spin glass $0.005 < \phi < 0.06$).

Glassiness in these magnetic systems could arise from different origins. On one hand, they exhibit low dimensionality, as already observed in low-dimensional molecule-based magnets.[44–46] On the other hand, the random distribution of spins in the network causes magnetic disorder and also promotes competing interactions. It is worth it to mention that the disorder is only magnetic. All synthesized compounds show well-defined X-ray diffraction patterns, and so they must be considered as polycrystalline solids and not as amorphous materials.

Calorimetry. In order to determine if the spontaneous magnetization in these materials arises from true (although glassy) magnetic ordering or from magnetic freezing of the system, specific heat measurements were performed by adiabatic calorimetry, using the standard heat-pulse method (Figure 11). All of the compounds show rounded anomalies with maxima (T_m) close to the maxima found in the ac susceptibility data. The absence of a λ peak (expected for a second-order phase transition) and the fact that, in all cases, T_m is higher than the corresponding temperature of the

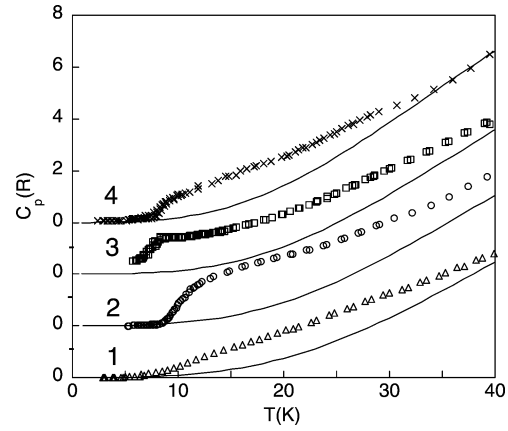

Figure 11. Specific heat data for **1**, **2**, **3**, and **4**. The data for **2**, **3**, and **4** have been shifted up for the sake of clarity. The phonon contributions have been estimated, as explained in the text.

susceptibility maximum confirms that long-range magnetic ordering is indeed not occurring in these systems, and therefore, they can be classified as spin glasses. X-ray diffraction spectra show diffraction peaks with a large width, which indicates a small grain size, estimated to be around 100−260 Å using Scherrer's formula. A predominant low-dimensional magnetic character combined with such a small crystal size could also give rise to the detected behavior masking the evidence of long-range magnetic ordering.

The estimation of the magnetic entropy requires the subtraction of the lattice contribution. The absence of a nonmagnetic isostructural compound forces us to roughly estimate this contribution using the heat capacity of compound **2** measured at higher temperatures (not shown in the figure). The data from 50 K up to 300 K have been adjusted with the appropriate Einstein and Debye functions, taking into account the collective modes and internal vibrations plus a Nerst−Lindemann term for the lattice expansion. The low-temperature phonon contribution ($T < 50$ K) calculated using these functions is drawn for compound **2** as a thin line in Figure 10. The lattice contribution for the other two compounds (also shown in Figure 11) has been obtained applying a corresponding state law in the 40−50 K temperature range. In the case of **1**, a similar procedure has been performed in order to estimate this lattice contribution, which is also drawn in the figure. The anomalous entropy calculated by integration of the heat capacity, once the lattice entropy has been conveniently subtracted, yields values below $S/R = \ln 12$. These values are far from the theoretical $S/R = \ln 54$, expected for the magnetic ordering of the spins of roughly two Ni^{II} ($S = 1$) and one Fe^{III} ($S = 5/2$) for **2**, **3**, and **4**. For compound **1**, the expected theoretical value $S/R = \ln 9$ is also higher than the experimental data, $S/R = \ln 4.5$. This could indicate that a non-negligible amount of entropy is already lost above 50 K and has not been considered with this lattice estimation. Still, a more plausible possibility is the fact that some magnetic disorder can still exist at the lowest temperature, and only part of the spins contribute to the magnetic entropy.

(43) Mydosh, J. A. In *Spin Glasses: An experimental introduction*; Taylor & Francis: London, 1993.
(44) Li, D. F.; Zheng, L. M.; Zhang, Y. Z.; Huang, J.; Gao, S.; Tang, W. X. *Inorg. Chem.* **2003**, *42*, 6123–6129.
(45) Min, K. S.; Rhinegold, A. L.; Miller, J. S. *Inorg. Chem.* **2005**, *23*, 8433–8441.
(46) Sharma, C. V. K.; Chusuei, C. C.; Clerac, R.; Moller, T.; Dunbar, K. R.; Clearfield, A. *Inorg. Chem.* **2003**, *42*, 8300–8308.

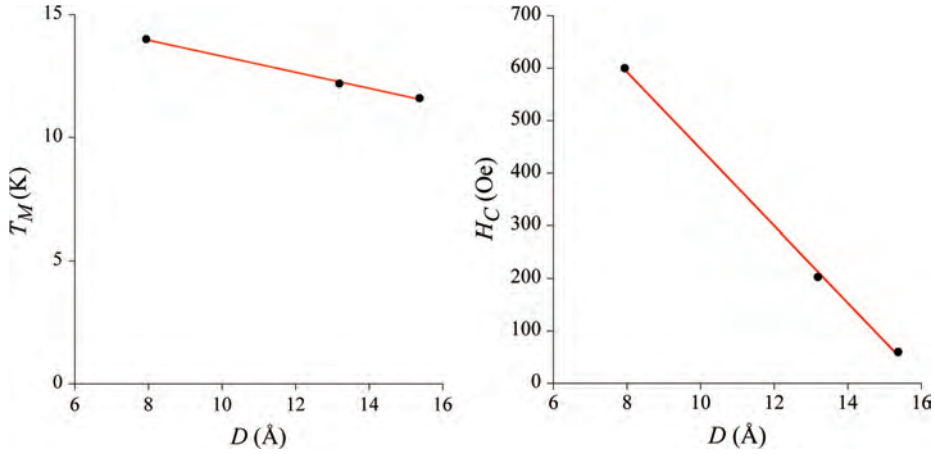

Figure 12. Relationship between spacing (D), spontaneous magnetization, and magnetic hysteresis in NiFe−NO_3 (**2**), NiFe−Adi (**3**), and NiFe−Seb (**4**).

Conclusion

We have been able to synthesize, in good yield and purity, polycrystalline layered double hydroxides with Ni^{II} and Fe^{III}, to study in detail their magnetic properties and the effect of dimensionality upon them. These materials showed the appearance of spontaneous magnetization at low temperatures, as a result of the magnetic interactions in the layers and in between the layers. Although no magnetic ordering is occurring, as demonstrated by magnetic and calorimetric measurements, the magnetic interactions between the randomly distributed metal ions make them behave as spin glasses. Indeed, the increase of the spontaneous magnetization is frequency-dependent, and it is not related to a second-order phase transition. Nevertheless, the freezing of these systems must be regarded as 3D, regardless of their quasi-2D magnetic structure, promoted by ferromagnetic interactions between the layers. Thus, the increase of the interlayer separation while maintaining identical magnetic structure in the hydroxide layers changes dramatically their magnetic behavior. The onset of the spontaneous magnetization happens at lower temperatures, and the magnetic hysteresis also becomes smaller as the spacer is larger. There are some further relaxation effects; the ac susceptibility shows more than one peak, but that should be related to domain movement, and actually only the higher-temperature peak corresponds to what is observed in the specific heat data.

The ferromagnetic nature of the interlayer interactions observed for all materials in this case is quite unique for this type of system. In the related layered hydroxides,[47,48] ferromagnetic interlayer interactions only appear for very long spacings, while antiferromagnetic interactions promote metamagnetic behavior for layered hydroxides with short spacings. Since the origin of the spontaneous magnetization is the same, on the basis of dipolar interactions between layers, we have found a relationship between the spacing and the magnetic properties. The temperature for the onset of spontaneous magnetization and the coercivity decrease linearly with D, at least in the range of spacers we tested (Figure 12). This shows that the magnetic properties in this type of material can easily be tuned.

In summary, we have shown here the remarkable and tunable magnetic properties of layered double hydroxides. The addition of spontaneous magnetization to the rich possibilities of LDHs can be very appealing for future development. The materials studied become magnets at very low temperatures and can be far from application at room temperature, but the rigidity of the brucite-like layers, which can be maintained when exchanging the metal ions, opens up the possibility of promoting stronger intralayer interactions, to reach higher freezing temperatures. Clays behaving as magnets at high temperatures could have many new applications, where magnetism could be combined with all of their remarkable properties.

Acknowledgment. This work was supported by the European Union (NoE MAGMANet) and the Spanish Ministerio de Educación y Ciencia (Project CSD2007-00010 Consolider-Ingenio in Molecular Nanoscience, and projects CTQ2005-09385-C03-01, CTQ2006-27186 and MAT2007-61621). A.R. and C.M.-G. thank the MEC for a Ramon y Cajal contract and for a PhD fellowship.

Supporting Information Available: IR and TGA data are available. This material is available free of charge via the Internet at http://pubs.acs.org.

IC801123V

(47) Laget, V.; Hornick, C.; Rabu, P.; Drillon, M. *J. Mater. Chem.* **1999**, *9*, 169–174.
(48) Rabu, P.; Drillon, M. *Adv. Eng. Mater.* **2003**, *5*, 189–210.